SRL Early Edition

EASTERN SECTION
SEISMOLOGICAL
RESEARCH LETTERS

Impact of Induced Seismicity on the Evaluation of Seismic Hazard: Some Preliminary Considerations

by Gail M. Atkinson, Hadi Ghofrani, and Karen Assatourians

ABSTRACT

A case study of seismicity induced by hydraulic fracturing operations near Fox Creek, Alberta, is used to evaluate the extent to which the potential for induced seismicity at a site alters the pre-existing hazard from natural seismicity. We find that in low-to-moderate seismicity environments, the hazard from an induced-seismicity source, if one is activated in close proximity to a site, can greatly exceed the hazard from natural background seismicity at most probabilities of engineering interest, over a wide frequency range. The most important parameters in determining the induced-seismicity hazard are the activation probability and the *b*-value of the initiated sequence. Uncertainty in the value of the key input parameters to a hazard analysis implies large uncertainty (more than an order of magnitude) in the likelihood of strong shaking.

INTRODUCTION

There has been a dramatic increase in the rate of seismicity in many parts of central North America in the last five to ten years, due to induced seismicity from oil and gas activity (Ellsworth, 2013). Most oil and gas operations do not trigger seismicity above the felt threshold; however, a small percentage of operations trigger events large enough to be felt (National Research Council [NRC], 2012), and an even smaller percentage trigger potentially damaging events. For example, events as large as **M** 5.7 are believed to have been triggered by deep disposal of fluids (Keranen *et al.*, 2013; Sumy *et al.*, 2014). The potential hazard from induced seismicity is a pressing issue, as in many parts of central and eastern North America (CENA) it may actually be the dominant source of seismic hazard. Seismic hazard from induced seismicity is inherently difficult to assess, because it is nonstationary, and new sequences are initiated regularly as resource development progresses. Moreover, the hazard may vary considerably with the parameters of the operation under consideration and the tectonic setting. In this article, we use a case study of seismicity induced by hydraulic fracturing operations near Fox Creek, Alberta, to explore some preliminary considerations for the assessment of seismic hazard from induced seismicity in CENA. In particular, we evaluate the extent to which the potential for induced seismicity at a site alters the pre-existing hazard from natural seismicity.

As with natural seismicity, the relative proportion of large to small events in an induced-seismicity sequence is governed by the *b*-value of the Gutenberg–Richter magnitude-recurrence law (Gutenberg and Richter, 1944). Thus, whenever an induced-seismicity sequence of small magnitude events is generated, there is a potential for larger events to occur, up to the maximum magnitude. Some studies suggest typical natural-seismicity *b*-values for induced seismicity (i.e., $b \sim 1$) if it becomes fracture driven (Goertz-Allmann and Wiemer, 2013). Other studies suggest steeper magnitude-recurrence slopes (i.e., $b \sim 2$), if the activity is occurring near the injection point as a response to the pore-pressure perturbation (Maxwell *et al.*, 2009; Wessels *et al.*, 2011). Once an induced-seismicity sequence is initiated, the *b*-value will be very important in determining the relative likelihood of larger events.

The maximum magnitude that might be triggered is also important in hazard assessment, particularly at lower probabilities. Some studies suggest that the maximum magnitude is limited by the volume of injected fluids (McGarr, 2014), while others suggest that it is limited only by the size of the fault upon which slip is initiated (Shapiro *et al.*, 2011). These two alternative estimates of maximum magnitude could be radically different in the case of operations with limited injected volume. For example, for a hydraulic fracture treatment operation, which by nature is of limited volume, one might infer a maximum moment magnitude (**M**) of about 4 (e.g., B.C. Oil and Gas Commission, 2012). On the other hand, if the maximum

doi: 10.1785/0220140204

magnitude is limited only by the available fault size, then its value would equal that for natural seismicity; this value is in the range of 6.5–7.5, even in the stable continental interior (e.g., Johnston, 1996a–c; Adams and Halchuk, 2003; Petersen *et al.*, 2008; Halchuk *et al.*, 2014).

In this article, we explore the impact of induced seismicity on hazard at a site in CENA near Fox Creek, Alberta. The site makes a good case study because it is in an area of previously low seismicity that suddenly became active in December 2013 and has since hosted dozens of events of $\mathbf{M} > 2.5$, with observed events as large as **M** 4.4. The presumed cause of the seismicity is hydraulic fracturing activity in the area that initiated at that time and is ongoing. It is noteworthy that there are no disposal wells nearby, and therefore large-volume injection wells are not a potential cause for the induced seismicity.

We first calculate the natural-seismicity hazard at a site in the immediate vicinity of the induced sequences as of 2013, before the induced activity commenced. We then show how the hazard is impacted by the addition of a small local source zone for the new induced activity (as of 2014), considering uncertainty in the parameters of the initiated sequence to explore the sensitivity of the hazard. We also address the broader question of similar sites at which there is currently no induced seismicity occurring but which may become the site of an induced-seismicity sequence in the future as resource development progresses.

SEISMIC HAZARD AT FOX CREEK FROM NATURAL SOURCES (2013)

We use the national seismic-hazard model of the Geological Survey of Canada (GSC), developed in 2013 for the 2015 National Building Code of Canada (Halchuk *et al.*, 2014), as the benchmark for the hazard prior to the commencement of the induced seismicity near Fox Creek. The source model is composed of broad regional zones, as shown in Figure 1. For this exercise, we follow the classic probabilistic seismic-hazard analysis (PSHA) methodology as originally developed by Cornell (1968), Cornell *et al.* (1971), and McGuire (1976), using the EqHaz software (Assatourians and Atkinson, 2013) for the calculations. We select a site in the middle of the area that is currently active. The baseline model from GSC is adopted without modifications and does not reflect any of the induced seismicity from 2013 to the present. Therefore our calculations will mirror those of the GSC for the 2015 hazard maps (as given in Halchuk *et al.*, 2014). We note that some of the regional events in the baseline seismicity prior to 2013 may have been induced, and therefore what has been termed the "natural seismicity hazard" actually may have been influenced by past induced events in the region. However, there are no previous historical seismicity clusters anywhere near Fox Creek, and thus any contributions to hazard from induced seismicity can be assumed negligible prior to 2013.

We consider two variations in the implementation of the seismic source model; in both cases we adopt the GSC magnitude-recurrence parameters and uncertainty estimates as given in Halchuk *et al.* (2014) for all zones. The GSC model, which they implement using the FRISK88 hazard software (a proprietary software product originally developed by Risk Engineering Inc.), assumes a uniform distribution of seismicity within each source zone. As an alternative, we also consider an implementation that uses the same magnitude-recurrence parameters but that distributes the activity spatially over the zones in a way that mirrors a smoothed version of the historical seismicity in the zone (Fig. 1). This smoothed-seismicity variation is similar to the approach used by the U.S. Geological Survey (USGS) in the U.S. National Seismic Hazard Maps (e.g., Petersen *et al.*, 2008). Because the overlay of the uniform and smoothed-seismicity models makes Figure 1 cluttered, we illustrate only the distribution for the smoothed-seismicity approach in this figure.

The ground-motion model, also adopted directly from the GSC national hazard model, is a three-equation suite that represents median motions and their epistemic uncertainty, for B/C boundary rock-site conditions (shear-wave velocity of 760 m/s), as described by Atkinson and Adams (2013). Aleatory variability is also included as specified in the GSC model. The Fox Creek site is near the boundary between active tectonics in western North America (WNA) and stable craton tectonics in CENA. There are thus two ground-motion prediction equation (GMPE) models employed, one for shallow crustal earthquakes in WNA and one for CENA. The zone in which the site is located draws from the western model, whereas the less-active regions to the east use the eastern model; the reader is referred to Halchuk *et al.* (2014) for details.

The uniform hazard spectrum (UHS) for Fox Creek, calculated using EqHaz and the GSC hazard model and considering natural seismicity as of 2013, is shown in Figure 2 for probabilities of exceedance of 1/2500 per annum (p.a.) and 1/10, 000 p.a. The UHS plots the mean-hazard values of the response spectrum (5% damped pseudoacceleration, horizontal component, on B/C site conditions) for the stated annual probability, at selected frequencies of vibration. We checked the UHS calculation at 1/2500 p.a. to ensure it matches the GSC calculation; the values agree within 1%, which is close agreement considering the different software employed. The building code uses the 1/2500 p.a. UHS, whereas the 1/10, 000 p.a. UHS is often used for design or evaluation of critical facilities.

To place the UHS in context, we show a few scenario events drawn from the median branch of the WNA GMPE suite, with one standard deviation added, in comparison to the UHS. We choose a median-plus-sigma GMPE level, because this is typically a strong contributor to hazard. The 1/2500 motions are similar to those expected from $\mathbf{M} \sim 6.5$ events at distances of ~100 km, and the 1/10, 000 motions are similar to those expected from $\mathbf{M} \sim 6.75$ events at distances of ~80 km. By comparison, moderate events ($\mathbf{M} \sim 5$) at close distances may cause stronger motions than these scenarios at high frequencies but much weaker motions at low frequencies (< 1 Hz).

We note that at Fox Creek the smoothed-seismicity model suggests lower hazard than does the uniform-seismicity model. This reflects the distribution of regional seismicity that can be seen in Figure 1; the Fox Creek region has experienced generally low activity rates to 2013. This also supports our earlier assertion that the contribution of induced seismicity to the

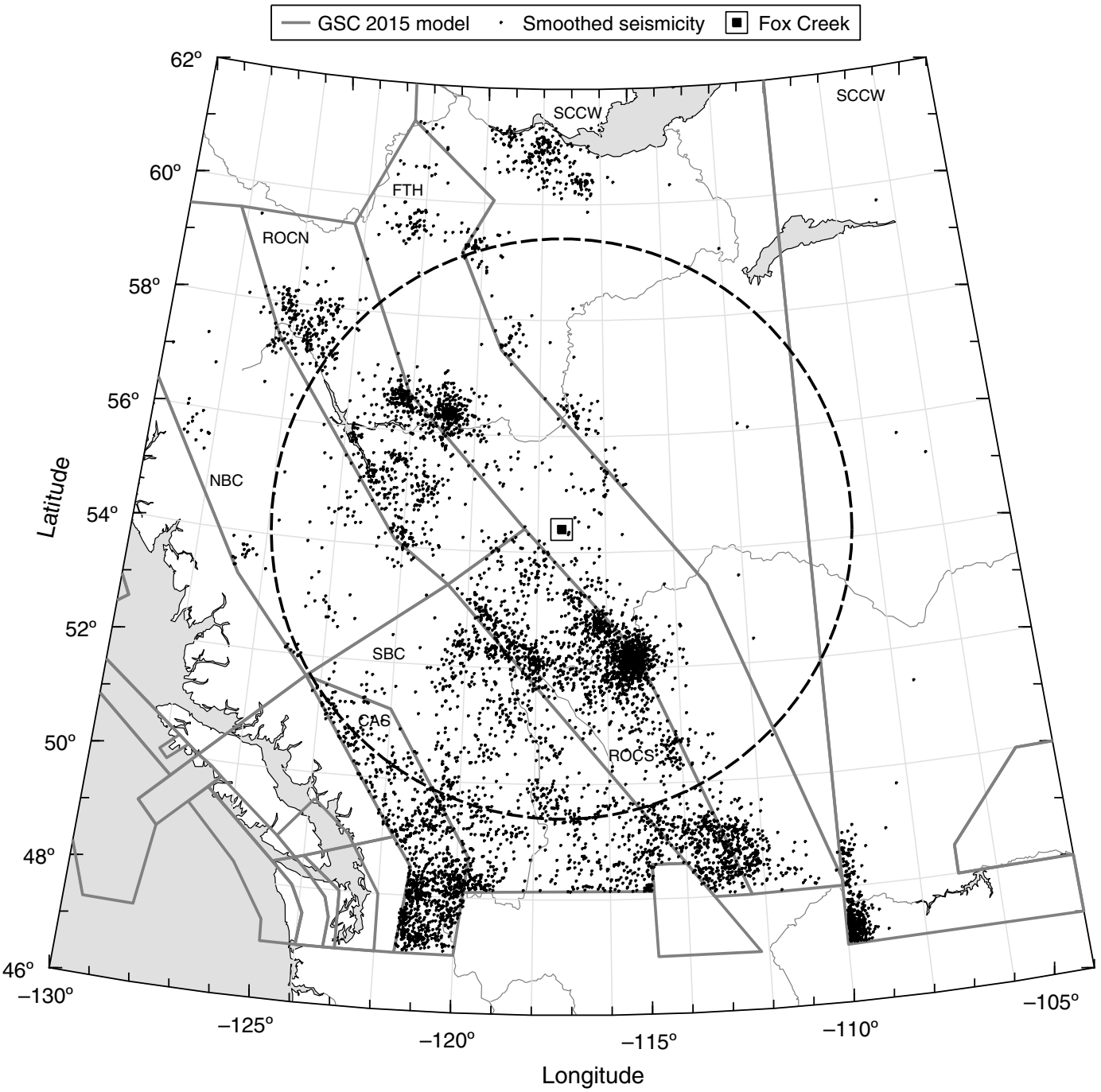

▲ **Figure 1.** Geological Survey of Canada (GSC) 2015 source zones around the Fox Creek area (delineated by lines). The dots show simulated events of **M** >3.5 for a 10,000-year catalog, based on the GSC magnitude-recurrence parameters (natural seismicity). Dots show the spatial distribution for the smoothed-seismicity approach; the dashed circle shows the 500 km radius around Fox Creek. The square shows the area in which the sequence occurred (2013–2014 seismicity not shown); the size of the filled inner square of the marker is about the size of the added source zone.

hazard, prior to 2013, is minimal. In the remainder of the article, we will use the smoothed-seismicity version of the natural-seismicity hazard calculations as the baseline for comparisons with the induced-seismicity hazard. We make this choice because we believe the smoothed-seismicity model to be more representative of the actual hazard levels indicated by the historical seismicity in the Fox Creek area.

SEISMIC-HAZARD MODEL AT FOX CREEK FROM INDUCED SEISMICITY (2014)

In December 2013, the seismicity rate at Fox Creek changed dramatically, when a sequence of events was initiated by hydraulic fracturing in the Montney formation. The hydraulic fracturing took place at a depth of about 2 km, which is the presumed depth

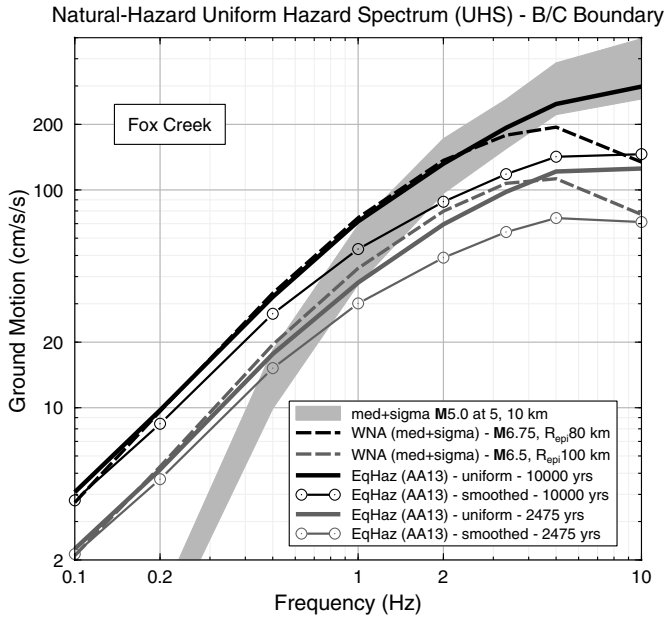

▲ **Figure 2.** The uniform hazard spectrum (UHS) for Fox Creek as of 2013 due to natural seismicity, for the return periods of 2500 years and 10,000 years. Results are shown for both the uniform-seismicity model (thick lines) and the smoothed-seismicity model (lines with circles). The expected motions (medium ground-motion prediction equation [GMPE] plus sigma) for several scenario events are shown for comparison: **M** 6.5–6.75 at 80–100 km (dashed lines); the range of motions for an event of **M** 5.0 at 5–10 km is shown by the shaded area.

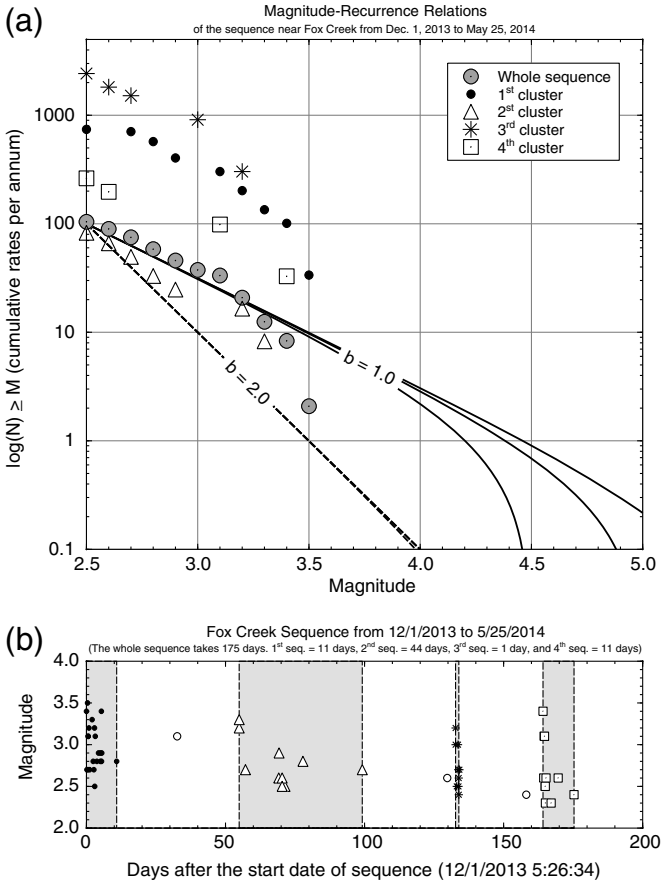

▲ **Figure 3.** Magnitude-recurrence parameters of the Fox Creek sequence, 1 December 2013 to 1 September 2014. (a) The bounded Gutenberg–Richter recurrence relations for $b = 1$ (solid lines) and $b = 2$ (dashed lines), considering $M_{max} = 4.5$ (lower), 5.0 (middle), and 5.5 (upper); for $b = 2$, these curves are indistinguishable. Rates have been normalized to per annum. (b) Recurrence behavior in time.

of the seismic activity; this also agrees with estimated depths from preliminary regional moment tensor analyses (A. Babaie Mahani, personal comm., 2015; W. Greig, personal comm., 2015). The details of the operations that induced the seismicity are just now starting to be released (information on hydraulic fracturing locations and volumes becomes public about 1 yr after the event). However, the sequence is known to have been frack induced, in part because there are no disposal wells or other plausible sources nearby and in part by the information currently available on the timing of the events in relation to hydraulic fracture operations that were taking place in the area. As of 1 September 2014, a total of 56 events of **M** ≥ 2 had occurred, with the largest event to that date being **M** 3.5. Moreover, in January 2015, after this study was completed, there were an additional 24 events of **M** ≥ 2 in the same area; six of the January 2015 events had **M** > 3, and the largest event, which occurred 23 January 2015, has an estimated M_L 4.4, at a depth of 2.1 km. The events were all located in a small area near Fox Creek, which we have represented as a new seismic source zone, whose extent is given approximately by the small (~10 km × 10 km) inner square in Figure 1 (latitude 54.355° to 54.445°, longitude −117.377° to −117.223°). We are considering the hazard for a site in the center of this activity. Thus it is important to recognize that the results will apply only to sites in very close proximity (within a few kilometers) to such operations.

Locations and magnitudes for the induced-seismicity source were obtained using catalog information from the TransAlta/Nanometrics seismographic network in Alberta (available at www.inducedseismicity.ca; last accessed March 2015) to September 2014; the moment magnitudes were calculated from the 1 or 3.3 Hz response spectral amplitudes using the algorithm of Atkinson *et al.* (2014). Figure 3 shows the magnitude-recurrence distribution of the seismicity, where the rates from 1 December 2013 to 1 September 2014 have been normalized to a per annum basis; moment magnitude (**M**) estimates are currently being refined for the events (Novakovic *et al.*, 2014), and the sequence is continuing, so the numbers of events at each M level, and the Gutenberg–Richter *b*-value, is currently uncertain. Figure 3 also shows how the activity occurred over time. The temporal plot is provided to illustrate the temporally clustered nature of activity, which is likely a result of it being induced by several hydraulic fracture operations, each of which initiated a sequence. It is obvious that the activity is nonstationary and thus not actually a Poisson process. In our evaluation of the impact of the activity

on hazard, we will first ignore this complication and consider a classic Poisson-model source zone having approximately the rates of activity indicated in Figure 3. Later, we will discuss the implications of the nonstationary aspects of the seismicity.

For our initial estimate of the induced-seismicity hazard, we use a loose interpretation of Figure 3 to assume that, in the new small source area that has been initiated, we have ~100 $\mathbf{M} \geq 2$ in a year. This is actually a lower bound on the rates in Figure 3, but we note that those rates have been normalized to a per annum basis. The assumed rate of 100 $\mathbf{M} \geq 2$ might be applicable if frequent operations in the area are expected to continue inducing seismicity at the rates observed in the last half-year. As of September 2014, one might have assumed that the b-value is quite steep, given the lack of observations of any $\mathbf{M} > 4$ events; for a typical b-value of 1, we would have expected five or more events of $\mathbf{M} \geq 3$ and might have seen an $\mathbf{M} \geq 4$ event. In the study time period, we observed more than five $\mathbf{M} > 3$ events but no events of $\mathbf{M} > 4$ in the sequence. However, as of January 2015, there is now an observed event of $\mathbf{M} > 4$. We examine the sensitivity of hazard for b values in the range from $b = 1$ to $b = 2$. Generally, $b = 2$ is considered plausible for induced-seismicity sequences in which the activity is being driven by the hydraulic fracture process, rather than being fracture driven; the b-value may also evolve over time and distance (Goertz-Allmann and Wiemer, 2013). We acknowledge that the Fox Creek sequence appears to be more consistent with a b value near 1, rather than 2, especially given the recent larger-magnitude seismicity occurring in the area. Our goal is not to fit a b-value to this particular activity. Rather, we aim to explore the implications of hydraulic fracturing on seismic hazard, using this sequence as an example. Thus we explore the implications of a range of b values from 1 to 2.

The maximum magnitude (M_{max}) for hydraulic fracture-induced events is not known; however, the largest observed event has increased over time, and thus any absolute maximum that may exist has probably not yet occurred. The largest such event observed to 2010 was an $\mathbf{M}$ 2.8 event near Blackpool, England (NRC, 2012). A significantly larger event ($\mathbf{M}$ 3.6) was induced in 2011 by hydraulic fracturing near Horn River, British Columbia (B.C. Oil and Gas Commission, 2012). As of 2013, the maximum was believed to be an event of $\mathbf{M}$ 4.3, also in British Columbia (D. Walker, personal comm., 2013). More recently, on 4 August 2014 a hydraulic-fracture-related event occurred near Fort St. John, British Columbia, that has a regional moment tensor magnitude in the range of $\mathbf{M}$ 4.1 (Atkinson *et al.*, 2014) to 4.4 (H. Kao, personal comm., 2014), and in January 2015 an event of $\mathbf{M} \sim 4.4$ occurred in the Fox Creek area. Based on these events, we take a value of $\mathbf{M} = 4.5$ as a lower bound on M_{max}. For the upper bound on M_{max}, we assume an event that is somewhat smaller than the maximum magnitude for natural events. We acknowledge that this is a judgement, because it is not actually known if the maximum magnitude for induced events is smaller than that for natural events. We weight the distribution toward low-to-moderate values of M_{max}; this, too, is a subjective judgement that we hope to be able to refine in the future when more information becomes available. We use a logic-tree format to represent the assumed probability distribution of M_{max} to input to the PSHA, with branch weights (w_i) as follows: $M_{max} = 4.5 (w_i = 0.4)$, $M_{max} = 5.0 (w_i = 0.3)$, $M_{max} = 5.5 (w_i = 0.2)$, and $M_{max} = 6.5 (w_i = 0.1)$. The weights are arbitrarily chosen for exploratory purposes. We note that more extreme scenarios for M_{max} have not been considered here—we are placing most of the weight toward the low end of the distribution, while allowing for some possibility that M_{max} could be as large as 6.5.

Minimum magnitude (M_{min}) values are also important to the computed hazard. A general empirical rule of thumb in the past has been that events of $\mathbf{M} < 5$ do not generally cause damage. However, this empirical rule is based on an implicit assumption of typical focal depths for natural events. Induced events are much shallower than natural events on average and may thus cause strong ground motions at close epicentral distances (Hough, 2014; Atkinson, 2015). It is not known what minimum magnitude might be capable of causing damage, and thus contributing to hazard, for these shallow events. Here, we consider values in the range from $M_{min} = 3.5$ to 4.5. This is based on observations that induced events of $\mathbf{M}$ 3.5 have caused damage to vulnerable structures (Giardini, 2009). We consider the source at an average depth of 2–5 km, weighted as follows: $h = 2$ km ($w_i = 0.3$), $h = 3$ km ($w_i = 0.4$), and $h = 5$ km ($w_i = 0.3$). The actual source depth is not well constrained, though it is close to 2 km for the most recent activity in the area.

GROUND-MOTION PREDICTION EQUATIONS (GMPES) FOR INDUCED-SEISMICITY SOURCE

Most GMPEs are not well suited for induced-seismicity applications, as they were not derived to adequately model amplitudes for moderate events at the very close hypocentral distances that result for shallow events. The suite used for the 2015 national hazard model of Canada is particularly deficient for such applications because the explanatory variable is R_{JB} (distance to the surface projection of the rupture), which cannot account well for the focal depth effects seen in induced-seismicity datasets. Therefore, for the induced-seismicity ground-motion model, we use the Atkinson (2015; referred as A15) GMPE developed for $\mathbf{M} < 6$ events at distances < 40 km, parameterized in hypocentral distance (R_{hypo}), as a backbone model for induced-event ground motions. We construct upper and lower branch models by considering its epistemic uncertainty in an analogous approach to that taken by Atkinson and Adams (2013) for the GSC national model, designated as AA13. This will provide a simple three-branch ground-motion model, consisting of a central, lower, and upper GMPE for median motions. The epistemic uncertainty is very significant at close distances (Atkinson, 2015), and thus the lower and upper GMPE curves will spread widely. At larger distances (where focal depth is unimportant), the amount of epistemic uncertainty should converge to that in the AA13 uncertainty model. It should be further noted that aleatory uncertainty is larger for induced events than for natural events, as discussed in Douglas *et al.* (2013) and Atkinson (2015).

The central GMPE of the induced-seismicity suite is the small **M** GMPE proposed in Atkinson (2015), which includes a near-distance saturation term as given by Yenier and Atkinson (2014). Atkinson (2015) also provides an alternative saturation term, discussed further below, which essentially provides an alternative central GMPE at close distances; there is no difference between the two alternatives given in Atkinson (2015) at distances >20 km. We define alternative branches (high, low) about these two variations on the central model that represent uncertainty in the best value for the median GMPE. To keep the alternative equations simple, we use the AA13 approach to define amounts to add and subtract from the two central GMPEs, in log units. We use the AA13 equation to get the initial uncertainty width in log units. We further assume that the AA13 upper and lower branches, relative to the central branch, give the correct overall amount of epistemic uncertainty for $R_{hypo} \geq 20$ km; we use this number of log units (0.15 units, or a factor of 1.4) to represent the epistemic uncertainty in the median GMPE for distances of 20 km and greater.

The size of the epistemic uncertainty band about the central GMPE (Fig. 4) depends on the degree to which the expected amplitudes can be constrained by empirical data. A key issue that is unresolved by current data is the amount of near-distance saturation for small-to-moderate events. Our default model (primary variant) for the central GMPE assumes the near-distance saturation model provided in Yenier and Atkinson (2014); this model assumes that amplitudes saturate fully only within a distance of $h_{eff} = 1$ km for events of $\mathbf{M} \leq 4$, increasing to a saturation distance of $h_{eff} = 7.2$ km at $\mathbf{M} = 6$. (h_{eff} is an effective-depth term that constrains the closest distance from the source to the observation point in an equivalent point source model.) In view of the possibility that the near-distance saturation is greater than that proposed by Yenier and Atkinson (2014), as discussed by Atkinson (2015), we consider the proposed alternative near-distance saturation function of A15, given by: $h_{eff} = \max(1, 10^{(0.28+0.19M)})$. The alternative saturation function has a value of $h_{eff} = 3$ km at $\mathbf{M} = 4$, increasing to match the value of $h_{eff} = 7.2$ km at $\mathbf{M} = 6$ that is given by the Yenier and Atkinson (2014) expression (equation 3 in Yenier and Atkinson, 2014). Overall, we assume that the A15 GMPE model is more likely to be conservative than unconservative and that the overall amplitude uncertainty at close distances is greater for small events; this is motivated by the lesser data constraints for $\mathbf{M} < 6$ events at very short hypocentral distances.

For near-hypocentral distances, we assume that the uncertainty bounds widen symmetrically to a magnitude-independent maximum factor of 2.0 about each of the two alternative central branches at $R = 1$ km. The uncertainty bounds reduce steadily with distance to the AA13 factor of 1.4 at 20 km, as shown in Figure 4. For distances from 1 to 20 km, the uncertainty factors are calculated from interpolation on the logarithmic scale between 2.0 and 1.4 (i.e., the log of uncertainty factor versus log of distance is assumed to be a straight line). We add the log-based uncertainty factor to the default-saturation (primary) central GMPE variant of A15 and subtract this factor from the alternative-saturation central GMPE variant of A15. This provides four GMPEs (two alternatives for the central curve, a low curve, and a high curve) that cover a wide range of potential median ground motions at close distance and small magnitudes.

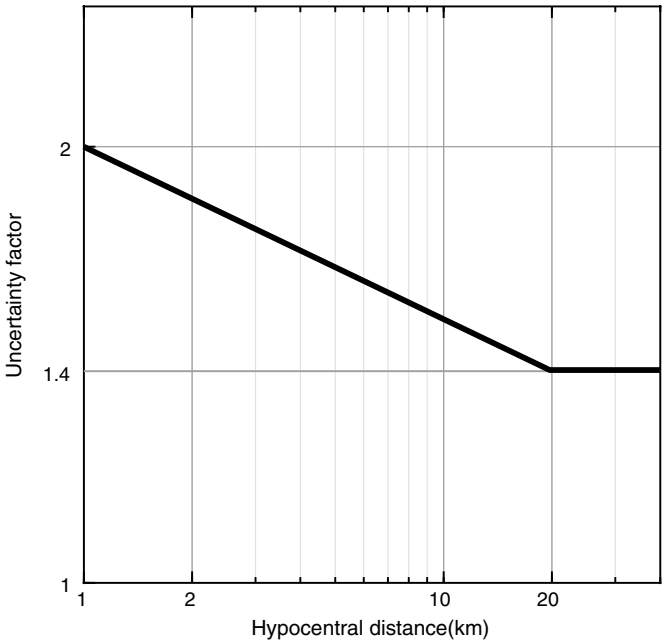

▲ **Figure 4.** Epistemic uncertainty model for the GMPE as a function of distance relative to the central model. This factor multiplies the central A15 GMPE variant with the Yenier and Atkinson (2014) saturation term and divides the central A15 GMPE variant with the alternative saturation term.

We apply the uncertainty factor as defined in Figure 4 to the two alternative central variants of the A15 GMPE to obtain the alternative GMPE branches to represent the total epistemic uncertainty in median motions, as shown in Figure 5. For comparison, Figure 5 also shows the range of amplitude estimates from the alternative Next Generation Attenuation (NGA)-West 2 GMPEs, and for the Atkinson and Adams (2013) central-branch GMPE used for the 2015 national hazard model; note the average focal depth is 9 km for the NGA-West 2 records. In our induced-hazard calculations, we give the two central GMPE variants weights of $w_i = 0.3$ each, with $w_i = 0.2$ on each of the low and high curves. This defines the ground-motion characterization model for the induced-seismicity source.

The small defined seismic source for the induced seismicity, along with its magnitude recurrence and ground-motion model parameters as described above, allows us to compute the seismic hazard at Fox Creek that results from the new seismic source. We use a classic PSHA, with the EqHaz software, for this purpose. We compute the hazard from this new source separately from that of the natural background hazard, so that we can compare the expected ground motions from the two sources of hazard. As noted previously, we assume that the new source follows a classic Poisson process for initial illustrations, and we examine the implications of nonstationarity later.

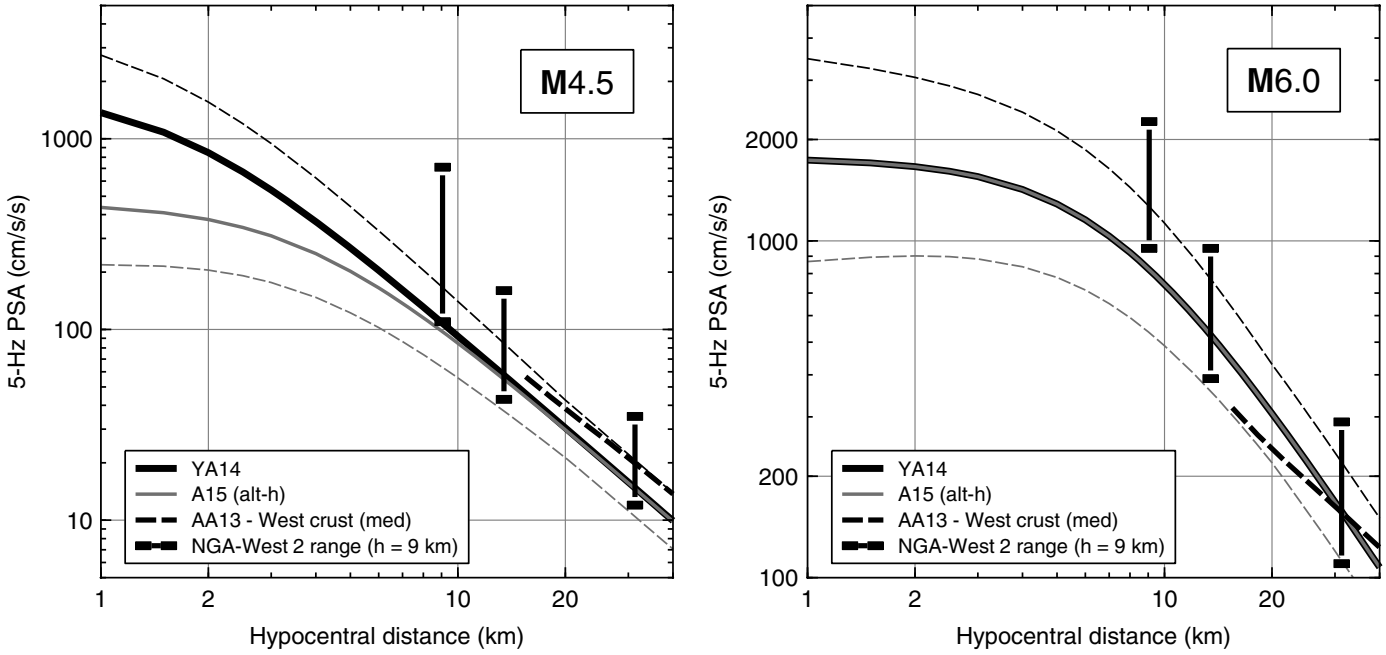

▲ **Figure 5.** Central GMPE variants (solid lines) and the upper and lower variants (dashed lines) for **M** 4.5 and **M** 6.0 events. The range of amplitude estimates from the alternative Next Generation Attenuation (NGA)-West 2 GMPEs (e.g., the range for natural-event motions) at hypocentral distance of ~9, 13, and 31 km is shown for each magnitude with solid vertical bars. The AA13 central-branch curves for the western crust are also shown; hypocentral distances <15 km are not shown for the AA13 curves due to their sensitivity to the conversion between R_{JB} and R_{hypo}.

RESULTS OF COMPARISON OF INDUCED-SEISMICITY TO NATURAL-SEISMICITY HAZARDS

In the following, we present the hazard curves for the induced-seismicity model in comparison to the corresponding curves for natural seismicity. First, we consider the case in which the induced-seismicity source that we defined has a 100% probability of being active (i.e., there is a 100% likelihood that this sequence occurs). The 100% probability of having the sequence describes the current hazard for an operation at Fox Creek that we know is causing seismicity, assuming that the activity continues. Then, we explore the impact of considering the initiation probability to be in the range from 1/100 to 1/1000. This corresponds to a situation in which new activities at a nearby location in the region might, or might not, trigger a sequence of this type. Note that changing the activation probability is equivalent to changing the seismicity rate parameter (Gutenberg–Richter *a*-value); the effective *a*-value will be the product of the rate parameter and the activation probability.

Figure 6 provides an overview of the induced-hazard curves (100% activation probability) in comparison to the corresponding curve for the natural-seismicity hazard (smoothed-seismicity model) at Fox Creek. Induced-hazard curves are shown for two Gutenberg–Richter *b*-values: $b = 1$ and $b = 2$. We consider a range of minimum magnitude values for the calculations, from 3.5 to 4.5, with the M_{max} logic-tree model as described in the previous section (i.e., M_{max} ranging from 4.5 to 6.5). As described previously, the induced events are assumed to occur at focal depths from 2 to 5 km. Figure 6 shows that if a sequence like that at Fox Creek is initiated, its ground motions at all probability levels of interest will clearly exceed those from the natural-seismicity hazard, at least for frequencies of 1 Hz and greater, PGA, and PGV. We caution that this statement is heavily conditioned upon the fact that Fox Creek has a low background level of natural seismicity. In areas of high natural seismicity, the relative impact of the induced seismicity source would be much less, because the natural-hazard curves would be at a much higher level.

The amplitude of the induced-seismicity hazard curve is highly dependent on the *b*-value of the sequence; a steep decay of event rates with increasing magnitude has a pronounced impact on the level of the hazard curves. The value of M_{min} is also important, especially at low-to-moderate levels of shaking, for steep *b*-values. This is because small-to-moderate events can cause significant shaking amplitudes. Research into the damage potential of high-amplitude motions from small-to-moderate events at very shallow depth would help determine what values of M_{min} are appropriate for practical applications.

In Figure 6, we assumed there is a 100% probability that the defined Fox Creek induced-seismicity source is active. For use in future applications for which we do not know if a sequence will be initiated, we explore the impact on results of assuming an initiation probability for such a sequence from 1/100 to 1/1000. For this sensitivity plot, we assume $M_{min} = 4.0$ and $b = 1$, with all other parameters fixed as in the previous example. As shown in Figure 7, the activation probability

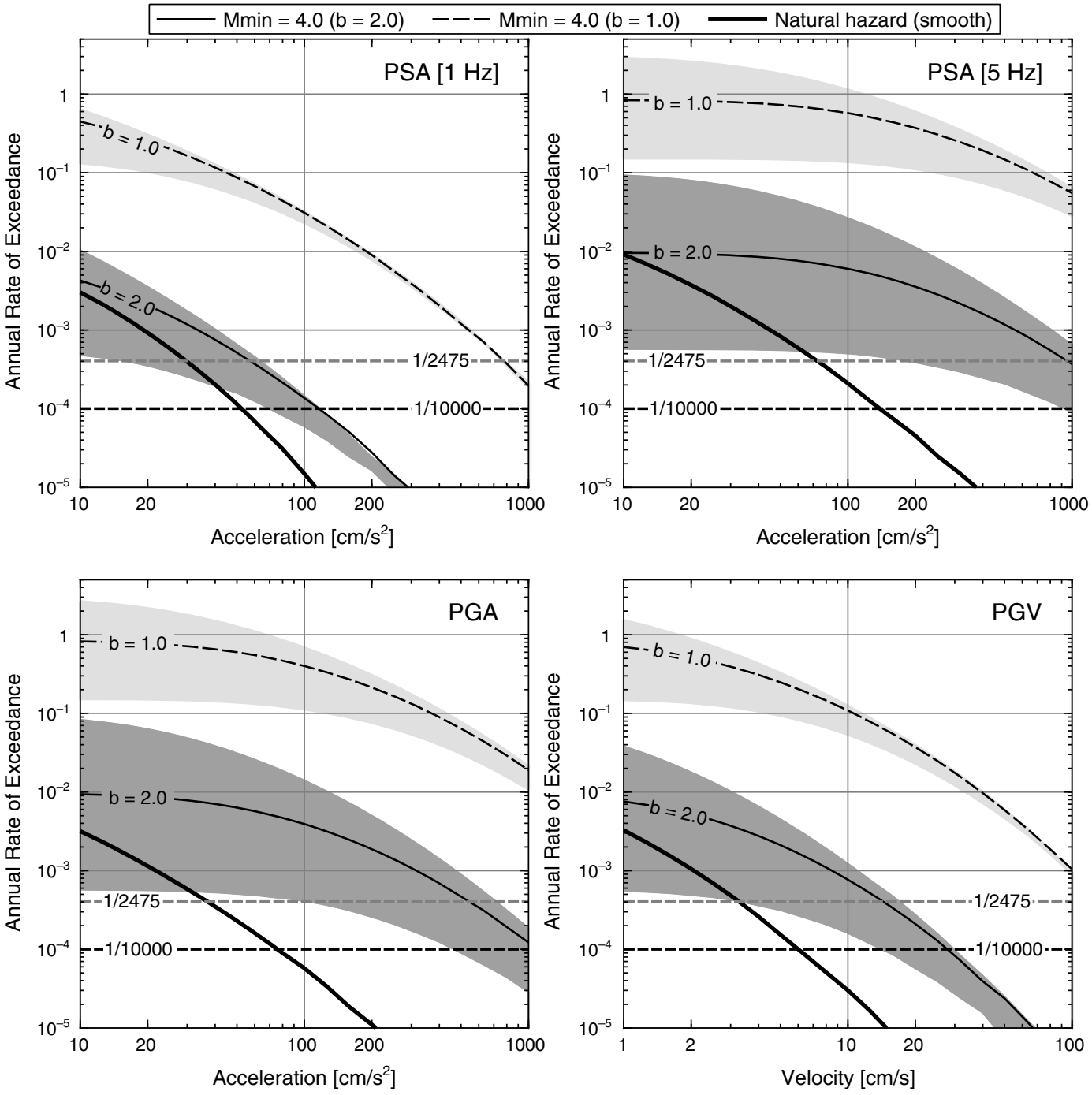

▲ **Figure 6.** Induced-seismicity hazard curves at Fox Creek calculated for $M_{min} = 3.5$ to 4.5 (shaded areas); the upper bound of the shaded area corresponds to $M_{min} = 3.5$, and the lower bound is for $M_{min} = 4.5$. Representative hazard curves for $M_{min} = 4.0$ are shown as a dashed line ($b = 1.0$) and as a solid line ($b = 2.0$). Results are shown for $b = 1.0$ (light gray shaded area) and $b = 2.0$ (dark gray shaded area).

is clearly an important parameter, which may impact the expected ground motions at probabilities of interest by as much as a factor of five (for sites like Fox Creek that are in a low-seismicity environment).

Figures 8 and 9 show the effects of the key sensitivities, M_{min} and b-value, on the mean-hazard UHS for typical probabilities of interest, 1/2500 and 1/10, 000 p.a. (for an activation probability of 0.01). As we would expect, the shape of the UHS is different for the induced-seismicity source than for the background natural seismicity. The induced-seismicity hazard is shifted toward higher-frequency content, due to the lower magnitudes and shorter distances that make up the contributions to hazard. This shift could be mitigated if the stress drops for induced events are less than those for natural earthquakes.

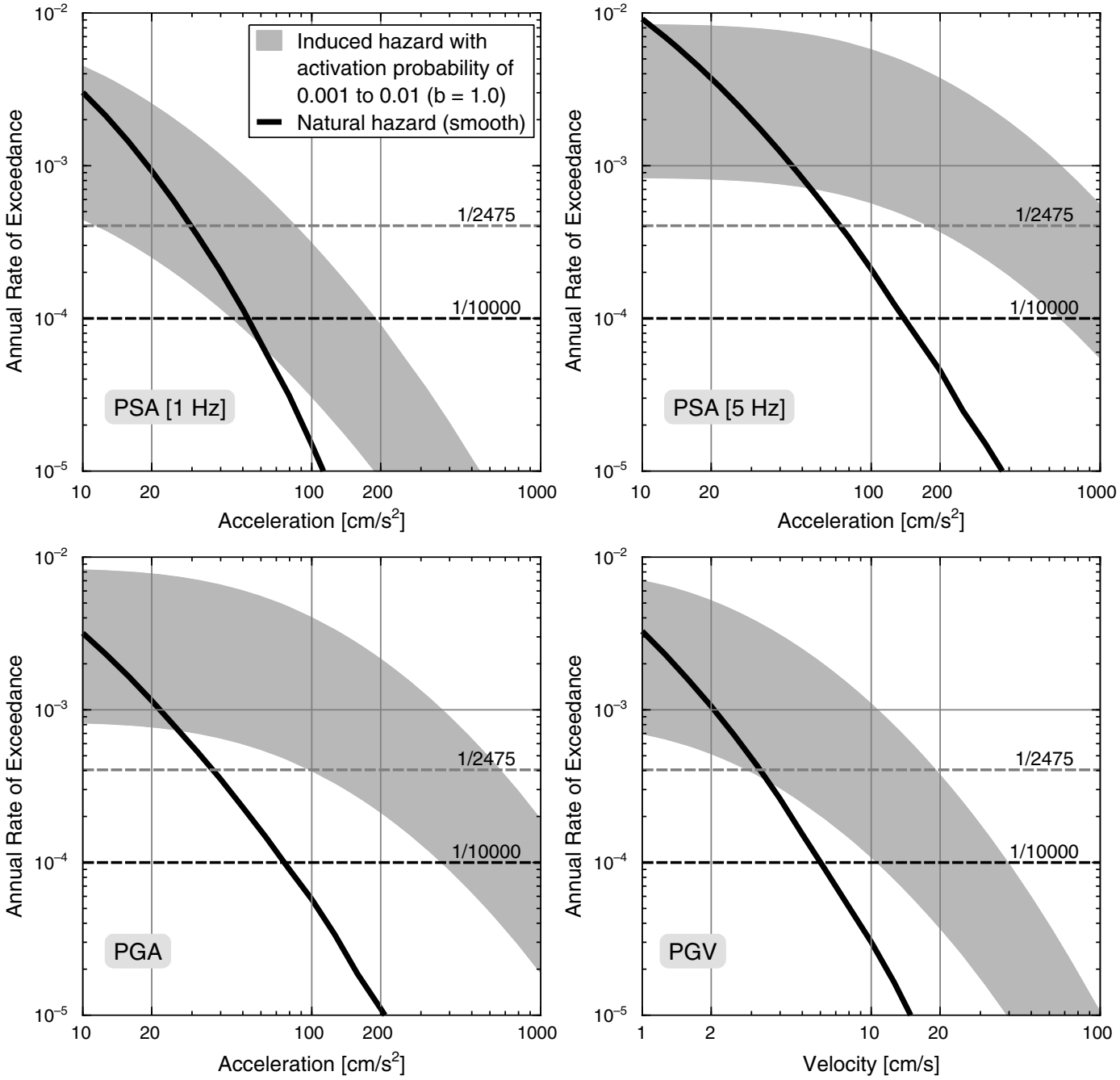

▲ **Figure 7.** Induced-hazard curves for $b = 1.0$ for activation probabilities in the range of 0.001 and 0.01 (shaded area) for $M_{min} = 4.0$.

If a lower stress drop can be documented for induced events, the high-frequency motions may be less than those shown, because our GMPE suite implicitly assumes that induced and natural events have the same average stress drop (Atkinson, 2015). However, Yenier and Atkinson (2014) report that stress drop scales with focal depth, with shallow events having lower stress drops. If the lower stress drop is purely a focal depth effect, then it is already at least partly accounted for in the Atkinson (2015) GMPE, by the use of hypocentral distance as the distance metric; this is because events at shallow depth control the GMPE at the shortest hypocentral distances.

From Figures 8 and 9, we conclude that the general effects of the parameters on the UHS are similar for the 1/2500 and 1/10,000 UHS. The b-value is the most important parameter, for a fixed activation probability. For b-values near 1, the UHS from the induced-seismicity source greatly exceeds the natural hazard, regardless of M_{min} (for M_{min} in the range from 3.5 to 4.5). For steep b-values, the hazard is greatly reduced, even for $M_{min} = 3.5$. It would be reduced even further for larger values of M_{min}, and thus M_{min} becomes important for steep b-values. We cannot plot the UHS for values of $M_{min} \geq 4$ for the $b = 2$ case for these return periods and activation probability, because

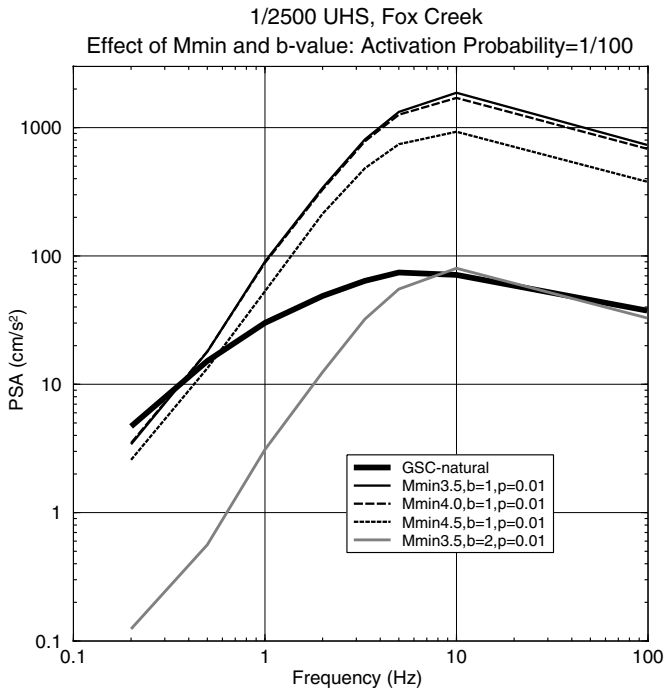

▲ **Figure 8.** Comparison of natural-seismicity mean-hazard UHS (smoothed seismicity) to induced-seismicity mean-hazard UHS, showing sensitivity to key induced-seismicity parameters M_{min} and b-value. The UHS is for 1/2500 per annum (p.a.) probability. The UHS cannot be calculated for M_{min} of 4.0 and greater for the $b = 2$, $p = 0.01$ case, because the event frequency becomes too low; this is due to the very small source defined in the exercise.

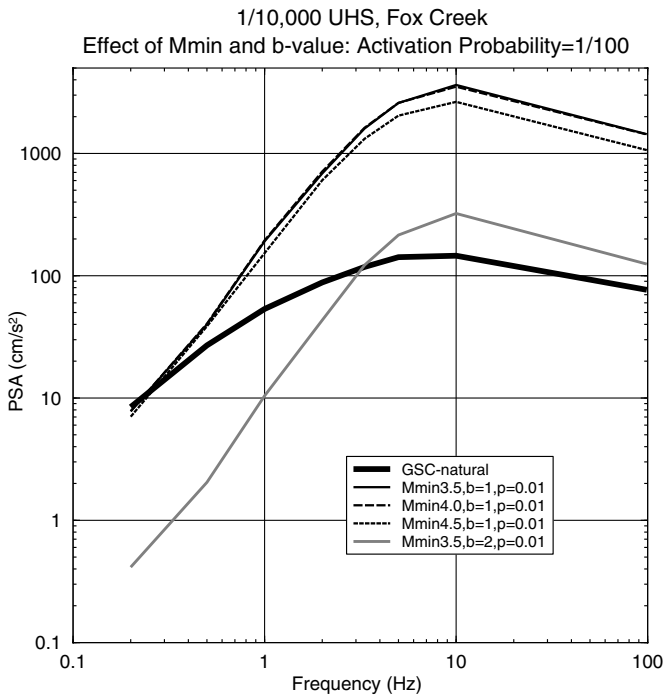

▲ **Figure 9.** Comparison of natural-seismicity mean-hazard UHS (smoothed seismicity) to induced-seismicity mean-hazard UHS, showing sensitivity to key induced-seismicity parameters M_{min} and b-value. The UHS is for 1/10,000 p.a. probability. The UHS cannot be calculated for M_{min} of 4.0 and greater for the $b = 2$, $p = 0.01$ case, because the event frequency becomes too low; this is due to the very small source defined in the exercise.

for the very small induced-seismicity source used in this exercise, the occurrence rate of events within the small source becomes too small. This means that there is effectively a lower limit on the ground-motion amplitudes for which the rates can be calculated.

In Figure 10, we examine the sensitivity of the UHS to M_{max}, for the $1/10,000$ p.a. probability, using the $M_{min} = 3.5$ case, for $p = 0.01$. (Results are similar for the $1/2500$ p.a. probability.) Interestingly, M_{max} is not that important unless $b = 1$. Thus the factors which are most important to the assessment of the hazard may vary significantly with the characteristics of the potential sequence that could be induced —especially its b-value and, of course, its activation probability.

IMPACT OF NONSTATIONARITY OF INDUCED-SEISMICITY HAZARD

In the preceding discussion, we made the simplifying assumption that we could treat the induced-seismicity sequence as a new seismic source that is similar to the background sources in that a sequence, once initiated, will follow a Poisson process. In reality, the activity is nonstationary in both space and time. The spatial aspects of the nonstationarity can perhaps be neglected by treating each potential sequence as a new small source zone. However, the temporal nonstationarity is a significant factor. One possibility is that the induced-seismicity sequence may follow an Omori-law type of decay sequence or follow some clustering model. Potential clustering models could include an epidemic-type aftershock sequence model (Ogata, 1988) to describe the temporal and spatial distribution of seismicity, fractal models (Kagan and Knopoff, 1980; Okubo and Aki, 1987), or multifractal models (Geilikman *et al.*, 1990; Hirata and Imoto, 1991; Hirabayashi *et al.*, 1992; Hooge *et al.*, 1994; Wang and Lee, 1996). Figure 11 illustrates the temporal behavior of the events. As an initial exercise, we attempted to fit the cumulative number of events to a modified Omori law as described by Utsu (Omori, 1894; Utsu, 1957; Utsu *et al.*, 1995). The fit of the sequences to this model is poor, which, not surprisingly, is based on an inspection of Figures 3 and 11. What we see instead are distinct clusters of activity, which are presumably related to individual fracking operations. We considered fitting each of the sequences individually; however, the event numbers are too sparse, and none of the sequences results in a good fit. Further work, with greater event numbers, is needed to understand the complex temporal behavior of these event sequences. At present, the data appear insufficient to better characterize the temporal behavior using models more complex than a simple Poisson model. To gain further insight into overall rate parameters, we can look at the apparent rates of

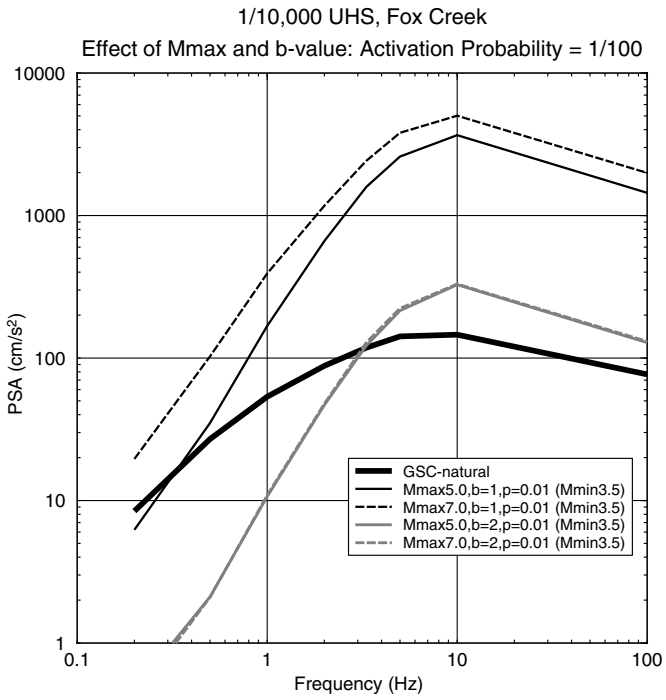

▲ **Figure 10.** Comparison of natural-seismicity mean-hazard UHS (smoothed seismicity) to induced-seismicity mean-hazard UHS, showing sensitivity to M_{max}. The UHS is for 1/10,000 p.a. probability (for $M_{min} = 3.5$ and $p = 0.01$).

seismicity within a sequence and make some further comments on the apparent likelihood of such sequences.

Based on Figure 3, for the period of time in which a sequence is active, the equivalent annual rate of occurrence of events of $\mathbf{M} > 3$ can exceed 1000. To obtain the effective annual rate, we need to multiply this by the activation probability, which is poorly known. To consider the activation probability in a broad context, we compared the number of horizontal wells that have been drilled (and presumably fracked) since the late 1980s, along with the number of earthquakes that have occurred, above a threshold magnitude of interest assumed to be **M** 3 in the large area of western Alberta shown in Figure 12. We use that information to approximate a preliminary regional activation probability. If we assume that about one in five events above the threshold were related to oil and gas (an arbitrary assumption), we obtain an overall regional activation probability of 0.001 (for $\mathbf{M} > 3$), resulting in an effective *a*-value of about 1 per annum (0.001 × 1000). This rate would imply that the likelihood of experiencing an event of $\mathbf{M} > 5$ in the sequence could be as high as 0.01 (on a per annum basis), for a *b*-value of 1. In contrast, in a very small area that encloses the cluster near Fox Creek, the activation probability for a sequence that includes $\mathbf{M} > 3$ events appears to be as high as 0.2, which would result in an effective a value of 500 (for $\mathbf{M} > 3$, normalized to a per annum basis). This high rate of induced seismicity would suggest that events of $\mathbf{M} > 5$ are relatively likely to occur due to hydraulic fracture activities in this environment, assuming that faults exist to host such events. Our conclusion is that in certain areas where the activation probability is high, the hazard may be greatly amplified by hydraulic fracturing activity. Even when the activation probability is modest (1 in 1000), the hazard contribution is still highly significant if the natural seismicity background is low to moderate.

In future work, we will develop alternative temporal process models for induced-seismicity sequences and explore their impact on hazard assessment. This will require compilation of

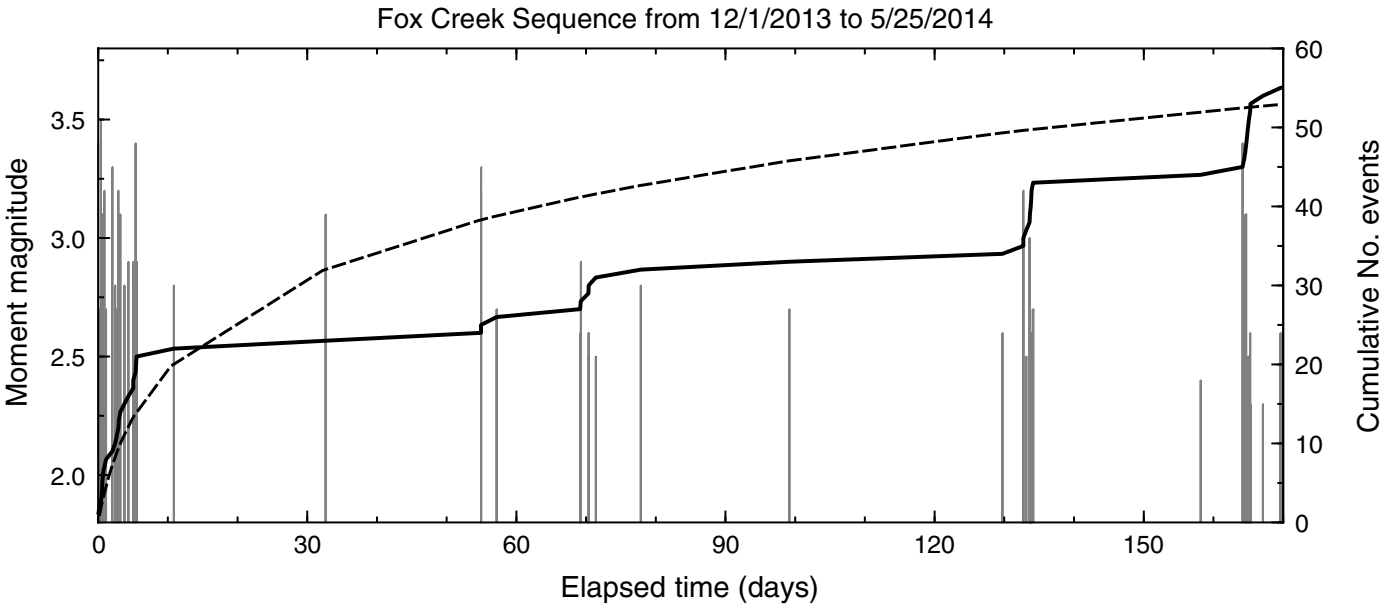

▲ **Figure 11.** Temporal distribution of seismicity in the Fox Creek area. Bars represent events with moment magnitudes recalculated following Atkinson *et al.* (2014), and the solid black line shows the cumulative number of events from the beginning of the sequence 1 December 2013 to 25 May 2014. The dashed black line is the fitted Omori model to the whole sequence.

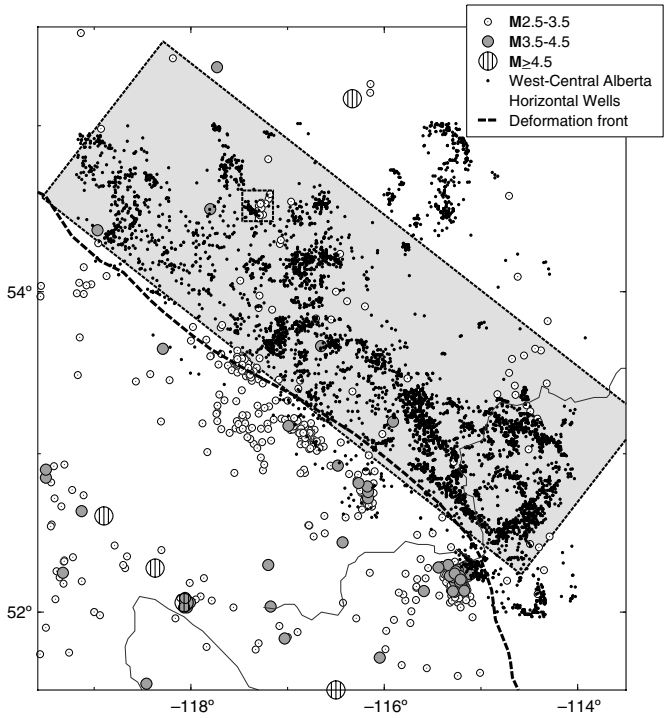

▲ **Figure 12.** Comparison between the number of events and the number of wells in the Fox Creek area (smaller box) and in a broader scale (larger box). Seismicity in the background is taken from the composite catalog to the end of 2013 (www.inducedseismicity.ca; last accessed March 2015). Small dots show surface location of horizontal wells in west-central Alberta since the late 1980s.

larger datasets, development of appropriate temporal models for such sequences, and modifications to the PSHA software to enable time-dependent hazard model calculations. We will also carry out further investigations to better understand the activation probability for induced-seismicity sequences. These developments are beyond the scope of the current study.

CONCLUSIONS

Several important conclusions can be drawn from the sensitivity analyses presented in this article.

1. In low-to-moderate seismicity environments, the hazard from an induced-seismicity source, if one is activated in close proximity to a site, can greatly exceed the hazard from natural background seismicity at most probabilities of engineering interest and over a wide frequency range.
2. The most important parameters in determining the induced-seismicity hazard are the activation probability and the b-value of the initiated sequence.
3. M_{max} (in the 4.5–6.5 range) is not critically important at most probabilities of interest unless $b \sim 1$. It should be noted that $b \sim 1$ for the Fox Creek dataset, and therefore M_{max} is important for this area.
4. M_{min} (in the 3.5–4.5 range) is not critically important at most probabilities of interest unless $b \sim 2$.
5. Uncertainty in the value of the key PSHA parameters implies large uncertainty (more than an order of magnitude) in the likelihood of strong shaking.

ACKNOWLEDGMENTS

Funding for this study from the Natural Sciences and Engineering Research Council of Canada and TransAlta is gratefully acknowledged. We thank Bill Ellsworth and an anonymous reviewer for their helpful comments, which led to significant improvements in the manuscript.

REFERENCES

Adams, J., and S. Halchuk (2003). Fourth generation seismic hazard maps of Canada: Values for over 650 Canadian localities intended for the 2005 National Building Code of Canada, *Geol. Surv. Canad. Open-File Rept. 4459*, 150 pp.

Assatourians, K., and G. M. Atkinson (2013). EqHaz—An open-source probabilistic seismic hazard code based on the Monte Carlo simulation approach, *Seismol. Res. Lett.* **84,** 516–524, doi: 10.1785/0220120102.

Atkinson, G. M. (2015). Ground-motion prediction equation for small-to-moderate events at short hypocentral distances, with application to induced seismicity hazards, *Bull. Seismol. Soc. Am.* **105,** no. 2A, doi: 10.1785/0120140142.

Atkinson, G. M., and J. Adams (2013). *Ground Motion Prediction Equations for Application to the 2015 Canadian National Seismic Hazard Maps*, http://www.seismotoolbox.ca/2012GMPEs.html (last accessed March 2015).

Atkinson, G. M., D. W. Greig, and E. Yenier (2014). Estimation of moment magnitude (M) for small events (**M** < 4) on local networks, *Seismol. Res. Lett.* **85,** 1116–1124, doi: 10.1785/0220130180.

B.C. Oil and Gas Commission (2012). *Investigation of Observed Seismicity in the Horn River Basin*, www.bcogc.ca (last accessed March 2015), 29 pp.

Cornell, C. A. (1968). Engineering seismic risk analysis, *Bull. Seismol. Soc. Am.* **58,** 1583–1606.

Cornell, C. A. (1971). Probabilistic analysis of damage to structures under seismic loads, in *Dynamic Waves in Civil Engineering: Proceedings of a Conference Organized by the Society for Earthquake and Civil Engineering Dynamics*, D. A. Howells, I. P. Haigh, and C. Taylor (Editors), John Wiley, New York, 473–493.

Douglas, J., B. Edwards, V. Convertito, N. Sharma, A. Tramelli, D. Kraaijpoel, B. Mean Cabrera, N. Maercklin, and C. Troise (2013). Predicting ground motion from induced earthquakes in geothermal areas, *Bull. Seismol. Soc. Am.* **103,** 1875–1897.

Ellsworth, W. L. (2013). Injection-induced earthquakes, *Science* **341,** doi: 10.1126/science.1225942.

Geilikman, M. B., T. V. Golubeva, and V. F. Pisarenko (1990). Multifractal patterns of seismicity, *Earth Planet. Sci. Lett.* **99,** 127–132.

Giardini, D. (2009). Geothermal quake risks must be faced, *Nature* **462,** 848–849, doi: 10.1038/462848a.

Goertz-Allmann, B. P., and S. Wiemer (2013). Geomechanical modeling of induced seismicity source parameters and implications for seismic hazard assessment, *Geophysics* **78,** KS25–KS39.

Gutenberg, R., and C. F. Richter (1944). Frequency of earthquakes in California, *Bull. Seismol. Soc. Am.* **34,** 185–188.

Halchuk, S., T. I. Allen, J. Adams, and G. C. Rogers (2014). Fifth generation seismic hazard model input files as proposed to produce values for the 2015 National Building Code of Canada, *U.S. Geol. Surv. Canada, Open-File Rept. 7576*, doi: 10.4095/293907

Hirabayashi, T., K. Ito, and T. Yoshii (1992). Multifractal analysis of earthquakes, *Pure Appl. Geophys.* **138,** 591–610.

Hirata, T., and M. Imoto (1991). Multifractal analysis of spatial distribution of microearthquakes in the Kanto region, *Geophys. J. Int.* **107,** 155–162.

Hooge, C., S. Lovejoy, D. Schertzer, S. Pecknold, J.-F. Malouin, and F. Schmitt (1994). Multifractal phase transitions: The origin of self-organized criticality in earthquakes, *Nonlinear Process. Geophys.* **1,** 191–197.

Hough, S. (2014). Shaking from injection-induced earthquakes in the central and eastern United States, *Bull. Seismol. Soc. Am.* **104,** 2619–2626.

Johnston, A. (1996a). Seismic moment assessment of earthquakes in stable continental regions—I. Instrumental seismicity, *Geophys. J. Int.* **124,** 381–414.

Johnston, A. (1996b). Seismic moment assessment of earthquakes in stable continental regions—II. Historical seismicity, *Geophys. J. Int.* **125,** 639–678.

Johnston, A. (1996c). Seismic moment assessment of earthquakes in stable continental regions—III. New Madrid 1811–1812, Charleston 1886 and Lisbon 1755, *Geophys. J. Int.* **126,** 314–344.

Kagan, Y., and L. Knopoff (1980). Spatial distribution of earthquakes: The two-point correlation function, *Geophys. J. Int.* **62,** 303–320.

Keranen, K. M., H. M. Savage, G. A. Abers, and E. S. Cochran (2013). Potentially induced earthquakes in Oklahoma, USA: Links between wastewater injection and the 2011 M_w 5.7 earthquake sequence, *Geology* **41,** 699–702, doi: 10.1130/G34045.1.

Maxwell, S., M. Jones, R. Parker, S. Miong, S. Leaney, D. Dorval, D. D'Amico, J. Logel, E. Anderson, and K. Hammermaster (2009). Fault activation during hydraulic fracturing, *79th Annual International Meeting, SEG*, Houston, 25–30 October 2009, Expanded Abstracts, 1552–1556.

McGarr, A. (2014). Maximum magnitude earthquakes induced by fluid injection, *J. Geophys. Res.* **119,** 1008–1019.

McGuire, R. K. (1976). FORTRAN computer program for seismic risk analysis, *U.S. Geol. Surv. Open-File Rept. 76-67*.

National Research Council (NRC) (2012). *Induced Seismicity Potential in Energy Technologies*, National Academy of Sciences, 300 pp.

Novakovic, M., G. Atkinson, and B. Cheadle (2014). Investigation of seismicity in the Crooked Lake region of Alberta, presented at *CGU Annual Meeting*, Banff, Alberta, 4–7 May 2014.

Ogata, Y. (1988). Statistical models for earthquake occurrence and residual analysis for point processes, *J. Am. Stat. Assoc.* **83,** 9–27.

Okubo, P. G., and K. Aki (1987). Fractal geometry in the San Andreas fault system, *J. Geophys. Res.* **92,** 345–355.

Omori, F. (1894). On the aftershocks of earthquakes, *J. Coll. Sci., Imperial Univ. Tokyo* **7,** 111–200.

Petersen, M., A. Frankel, S. Harmsen, C. Mueller, K. Haller, R. Wheeler, R. Wesson, Y. Zeng, O. Boyd, D. Perkins, N. Luco, E. Field, C. Wills, and K. Rukstales (2008). Documentation for the 2008 update of the United States National Seismic Hazard Maps, *U.S. Geol. Surv. Open-File Rept. 2008-1128*, 61 pp.

Shapiro, S. A., O. S. Kruger, C. Dinske, and C. Langenbruch (2011). Magnitudes of induced earthquakes and geometric scales of fluid-stimulated rock volumes, *Geophysics* **76,** WC55–WC63.

Sumy, D. F., E. S. Cochran, K. M. Keranen, M. Wei, and G. A. Abers (2014). Observations of static Coulomb stress triggering of the November 2011 M 5.7 Oklahoma earthquake sequence, *J. Geophys. Res.* **119,** 1904–1923, doi: 10.1002/2013JB010612.

Utsu, T. (1957). Magnitude of earthquakes and occurrence of their aftershocks, *Zisin* **10,** 35–45 (in Japanese).

Utsu, T., Y. Ogata, and R. S. Matsu'ura (1995). The centenary of the Omori formula for a decay law of aftershock activity, *J. Phys. Earth* **43,** 1–33.

Wang, J.-H., and C.-W. Lee (1996). Multifractal measures of earthquakes in west Taiwan, *Pure Appl. Geophys.* **146,** 131–145

Wessels, S., M. Kratz, and A. D. L. Pena (2011). Identifying fault activation during hydraulic stimulation in the Barnett shale: Source mechanisms, b values, and energy release analysis of microseismicity, *81st Annual International Meeting, SEG*, San Antonio, Texas, 18–23 September 2011, Expanded Abstracts, 1463–1467.

Yenier, E., and G. M. Atkinson (2014). Point-source modeling of moderate-to-large magnitude earthquakes and associated ground-motion saturation effects, *Bull. Seismol. Soc. Am.* **104,** 1458–1478, doi: 10.1785/0120130147.

Gail M. Atkinson
Hadi Ghofrani
Karen Assatourians
Department of Earth Sciences
Western University
London, Ontario
Canada N6A 5B7
gmatkinson@aol.com
hghofra@uwo.ca
kassatou@uwo.ca

Published Online 18 March 2015